European Journal of Soil Science

European Journal of Soil Science, January 2019, **70**, 162–173 doi: 10.1111/ejss.12729

Special issue article

Multi-sensor fusion for the determination of several soil properties in the Yangtze River Delta, China

D. Xu[a], R. Zhao[a], S. Li[a], S. Chen[b,c], Q. Jiang[a,d], L. Zhou[a] & Z. Shi[a,e]

[a]*Institute of Agricultural Remote Sensing and Information Technology Application, College of Environmental and Resource Sciences, Zhejiang University, Hangzhou 310058, China,* [b]*INRA, Unité InfoSol, 45075 Orléans, France,* [c]*UMR SAS, INRA, Agrocampus Ouest, 35042 Rennes, France,* [d]*College of Information Engineering, Tarim University, Alar 843300, China, and* [e]*Key Laboratory of Spectroscopy Sensing, Ministry of Agriculture, Hangzhou 310058, China*

Summary

Soil organic matter (SOM), total nitrogen (TN), available nitrogen (AN), available phosphorus (AP), available potassium (AK) and pH are key chemical properties for evaluating soil fertility and quality. This study involved the integration of four soil sensors, visible near-infrared (vis–NIR) spectrometer, mid-infrared (mid-IR) spectrometer, portable X-ray fluorescence (PXRF) analyser and laser-induced breakdown spectroscopy (LIBS), to achieve rapid measurement of these soil properties. A genetic algorithm and partial least-squares regression (GA–PLSR) were used to select characteristic bands to reduce data redundancy. We then calibrated models from three aspects: models using partial least-squares regression (PLSR) based on single sensor data, models using PLSR based on fused sensor data, involving data combined from the four sensors into a new dataset to create a data fusion (DF) model, and models with Bayesian model averaging (BMA) based on prediction results of fused sensor data, involving prediction results combined from the four sensors into a new dataset to form the BMA model. The results showed the following. (i) For the single sensor, the predictive performance decreased as follows: mid-IR > vis–NIR > LIBS > PXRF. (ii) Compared with the single sensor approach, the DF approach slightly improved or even reduced prediction accuracy and caused a large amount of redundancy. We suggest that this approach is not able to improve predictive ability. (iii) The BMA approach achieved the best prediction for the six soil properties. Our findings suggest that model averaging of vis–NIR, mid-IR and LIBS could be a reliable and stable approach for the fast measurement of soil properties.

Highlights

- We used four proximal soil sensors to evaluate six key properties for evaluating soil fertility and quality.
- GA–PLSR was used to select characteristic bands.
- We compared predictions of six soil properties from single sensor, DF and BMA approaches.
- BMA predictions were more accurate than predictions from single and fused sensor data.

Introduction

As a major soil type, paddy soils are widely distributed in China with an area of about 30 million hm^2, which accounts for 29% of cultivated land in China, especially in the Yangtze River Delta and South China (Li, 1992). Paddy soil is also affected considerably by human activities. Since the 1980s there have been large inputs of chemical fertilizers to Chinese arable land, which has caused a direct or indirect decrease in soil pH. Moreover, too much N fertilizer has also affected soil acidification both directly and indirectly (Guo *et al.*, 2010). It is necessary to determine information about soil properties that are related to soil fertility to be able to conduct variable-rate fertilizer application. Soil organic matter (SOM), as the important source for various nutrient elements in soil, is an essential factor for estimating soil fertility (Zhou *et al.*, 2016). Soil

Correspondence: L. Zhou. E-mail: lianqing@zju.edu.cn
Received 29 October 2017; revised version accepted 5 August 2018

total nitrogen (TN) is another indicator of soil fertility and quality, and in addition available nitrogen (AN), available phosphorus (AP) and available potassium (AK) are closely related to plant growth and have a great effect on fertilizer recommendation (Miller & Gardiner, 1998). Thus, fast, timely and accurate determination of these soil properties in paddy soils, because of their economic importance, is essential for agricultural production and ecological protection.

A variety of agricultural sensors has been applied over recent decades to determine soil properties rapidly (Gebbers & Adamchuk, 2010). Spectroscopy, in particular, has increased in popularity because it is rapid, timely, cost-effective, non-destructive and straightforward (Li *et al.*, 2015; Ji *et al.*, 2016; Xu *et al.*, 2018). As effective alternatives to traditional chemical analysis, vis–NIR, mid-IR and combined diffuse reflectance spectroscopy have the potential to predict various soil properties simultaneously (Viscarra Rossel *et al.*, 2006; Viscarra Rossel & Webster, 2012). Therefore, vis–NIR and mid-IR have long drawn the attention of pedologists.

Recently, portable X-ray fluorescence spectroscopy (PXRF) has become increasingly popular for its large sample throughput and minimal sample preparation (Zhu *et al.*, 2011). In general, PXRF is applied for determining heavy metal contamination of soil (Hu *et al.*, 2017). Moreover, elemental data determined with PXRF have been used as an alternative to the measurement of soil texture and pH (Zhu *et al.*, 2011; Sharma *et al.*, 2014).

Laser-induced breakdown spectroscopy (LIBS), a kind of atomic emission spectroscopy, performs relatively rapid analysis and can detect elements of both low and high atomic number simultaneously with minimal sample preparation (Samek *et al.*, 2006). Moreover, LIBS has been used in various applications such as the analysis of soils and marine sediments. In soil research, LIBS is used mainly for the analysis of heavy metal concentrations (Santos *et al.*, 2009). Recently, researchers have attempted to determine soil texture and soil organic carbon with LIBS (Villas-Boas *et al.*, 2016; Knadel *et al.*, 2017).

Many studies have been conducted on the use of single sensors to evaluate soil attributes. However, sometimes the prediction of soil properties with single sensors is less stable because of the complex nature of soil (Wang *et al.*, 2013). Thus, researchers have attempted to use data fusion from multiple sensors for prediction. Wang *et al.* (2013) predicted soil texture by integrating NIR and PXRF spectrometry and found that data fusion achieved a more accurate result than single sensors. Wang *et al.* (2015) characterized total carbon and total nitrogen by the synthesized use of vis–NIR and PXRF and obtained a more stable and solid result than with single sensors. O'Rourke *et al.* (2016) used vis–NIR and PXRF to determine agronomic soil properties and concluded that using model averaging techniques improved or maintained the status of predictions. Previous studies combined two (vis–NIR and mid-IR or vis–NIR and XRF) or three sensors (vis–NIR, mid-IR and XRF) to predict soil properties by using either sensor data fusion or model averaging (Viscarra Rossel *et al.*, 2006; Wang *et al.*, 2015; O'Rourke *et al.*, 2016). The study of fusion from four sensors (vis–NIR, mid-IR, XRF and LIBS) based on fusion of the sensor data and the sensor prediction results has not been done yet.

In this study, we integrated vis–NIR, mid-IR, PXRF and LIBS spectra for the determination of soil pH, SOM, TN, AN, AP and AK. The aims of this study were as follows: (i) compare the ability of vis–NIR, mid-IR, PXRF and LIBS to predict separately and (ii) compare the prediction capability of data from single sensors with that of data from multiple sensors, following two approaches. In the first approach data from the different sensors are merged, (including pairwise combination and the combination of three or four sensors) followed by application of partial least-squares regression (PLSR) to perform the prediction. This approach is referred to as the data fusion (DF) approach. In the second approach predictions from the separate sensors are combined into a single prediction outcome using Bayesian model averaging. This approach is referred to as the BMA approach.

Materials and methods

Study site and soil sampling

The study area covers 1831 km^2 and is located in Fuyang, in the southern part of the Yangtze River Delta, Zhejiang Province, China, with latitudes ranging from 29°44′N to 30°11′N and longitudes from 119°25′E to 120°19′E (Figure 1). The region has a subtropical monsoon climate with an average annual rainfall of approximately 1487 mm and an average annual temperature of 17.8 °C. The main soil type of this area is paddy soil, a type of Anthrosol in the Chinese soil taxonomy. The cultivated land was first extracted from the remote sensing data of land use in China (http://www.resdc.cn/data.aspx?DATAID=99). The cultivated land area was sampled on a square grid with a spacing of 1000-m for land that is far away from the town; for land near the town, the spacing was 400-m. Finally, a total of 301 sample sites were selected in cultivated land, and for each site, five individual topsoil samples (0–20 cm) were taken. These five samples were bulked to obtain a composite soil sample for each site. The soil samples were air-dried, stones and roots were picked out, and then the samples were ground and sieved to less than 2 mm in the laboratory prior to further analysis.

Chemical analysis

The SOM content was measured by the H_2SO_4–$K_2Cr_2O_7$ oxidation method at 180 °C for 5 minutes (Soil Science Society of China, 2000). Soil pH was determined at 1:1 soil:water suspension. Soil TN content was measured by the semi-micro Kjeldahl method and soil AN was measured by the alkaline hydrolysis diffusion method. Soil AP was measured by the NH_4F–HCl method (acid soil) or $NaHCO_3$ method (neutral or calcareous soil). Soil AK was measured by the NH_4OAc extraction method (Bao, 1981).

Spectral measurements and pre-processing

For the measurement of vis–NIR, mid-IR and PXRF spectra, the soil samples were spread on a culture dish, 5-cm diameter and 1-cm high, and flattened before scanning. For LIBS measurement, the

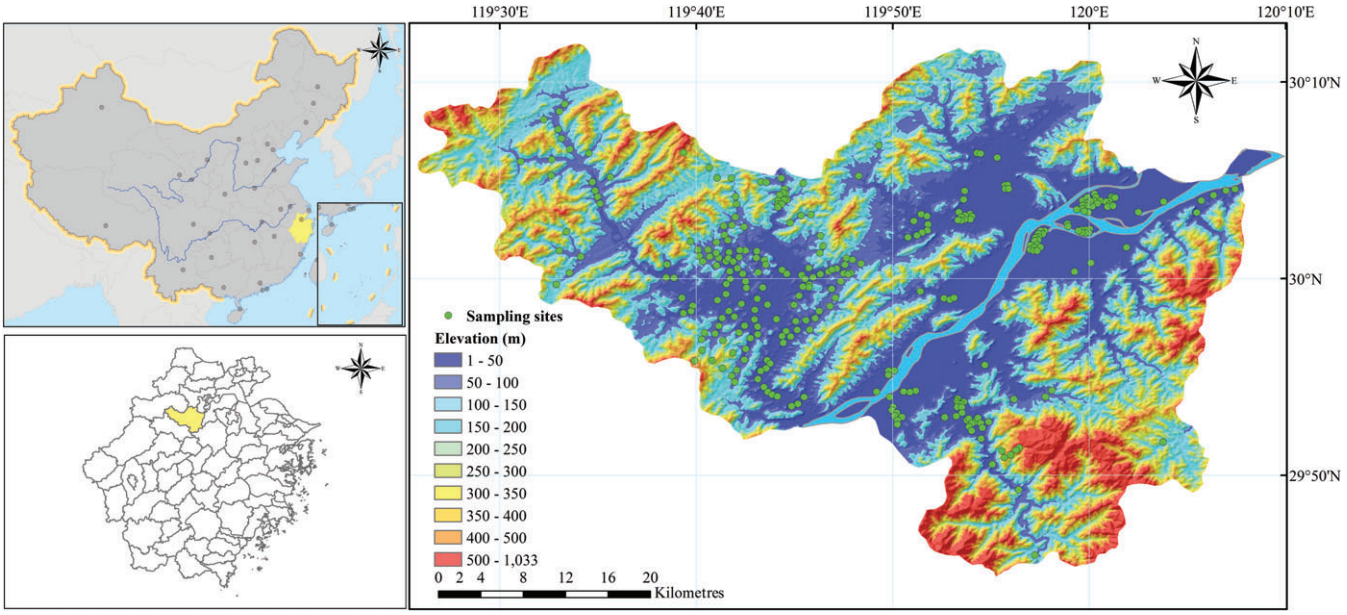

Figure 1 Maps showing the location of the study site and sampling sites. [Colour figure can be viewed at wileyonlinelibrary.com].

soil samples were made into cylindrical pellets with a diameter of 25 mm and a thickness of 3 mm using a manual pellet presser (FY-24, SCJS Co., Ltd, Tianjin, China) to obtain a homogeneous surface of the soil for measurement.

vis–NIR spectral measurement. The vis–NIR spectra of soil samples were measured with a Fieldspec® ProFR vis–NIR spectrometer (Analytical Spectral Devices, Boulder, CO, USA). The spectral range was from 350 to 2500 nm. The instrument has a spectral resolution of 3 nm between 350 and 1000 nm, and a spectral resolution of 10 nm between 1000 and 2500 nm. The sampling resolution of the spectra was 1 nm. Before each measurement, a Spectralon® panel with 99% reflectance was used to calibrate the spectrometer. Then the soil samples were measured using a high-intensity contact probe (Analytical Spectral Devices) with its own light source. Three random measurements were made at different positions in the dish. For each measurement, the instrument carried out 10 internal scans to obtain a satisfactory signal-to-noise ratio. A total of 30 spectra were averaged into one spectrum to represent that sample.

mid-IR spectral measurement. The mid-IR spectra of soil samples were measured with an Agilent 4300 Handheld FTIR (Fourier Transform Infra-Red) (Agilent Technologies, Santa Clara, CA, USA) with a spectral range of 4000–650 cm^{-1}. It has a DTGS (deuterated triglycine sulphate) detector with a spectral resolution of 4 cm^{-1}. Similarly, three random measurements were made at different positions in the dish and each soil spectrum was obtained by the mean of three replicated scans.

PXRF spectral measurement. The PXRF spectra were recorded with a Thermo Fisher Scientific Niton™ analyser (Thermo Fisher Scientific Inc., Billerica, MA, USA). Before measurement, the instrument was calibrated against a background and this was done every 30 samples. We selected the 'Soils Mode', and each sample was scanned three times for 90 s each time. Finally, the average of the three parallel scans was calculated as the result for the sample.

LIBS spectral measurement. The LIBS spectra were obtained by an assembly platform: a Q-switched Nd:YAG laser (Vilte-200, Beamtech Optronics Co., Ltd, Beijing, China), a high resolution Echelle spectrometer (Mechelle 5000, Andor Technology Ltd, Belfast, United Kingdom) coupled to an intensifier charge coupled device camera (iStar DH340T–18F–03, Andor Technology Ltd), a delay generator (DG645, Stanford Research Systems, Inc., Sunnyvale, CA, USA), an X-Y-Z moving stage (Zolix Instruments Co. Ltd, Beijing, China) and a personal computer with the Andor SOLIS software (Version 4.25, Andor Technology).

Pre-processing of spectra. For the vis–NIR spectra, the spectral regions of 350–399 nm and 2451–2500 nm were removed to eliminate the influence of noise. Because the spectra are highly collinear, the vis–NIR and mid-IR spectral data were down-sampled to a resolution of 10 nm and 8 cm^{-1}, respectively (i.e. the data were averaged within an interval of 10 nm and 8 cm^{-1}). Reflectance spectra were then transformed to apparent absorbance ($\log_{10}$ (1/R), where R is reflectance). To reduce noise further and to enhance the signals, spectra were smoothed using the Savitzky–Golay algorithm (SG; Savitzky & Golay, 1964), with a window size of 15 and polynomial of order 2.

There is currently no widely established approach for the pretreatment of PXRF spectra. Several pre-processing methods were tested, including the SG algorithm and standardization. The SG algorithm with a window size of 13 and polynomial of order 2 was selected because it produced the best model performance. The XRF spectra were also down-sampled to a resolution of 0.15 keV and LIBS spectra were down-sampled to a resolution of 1 nm.

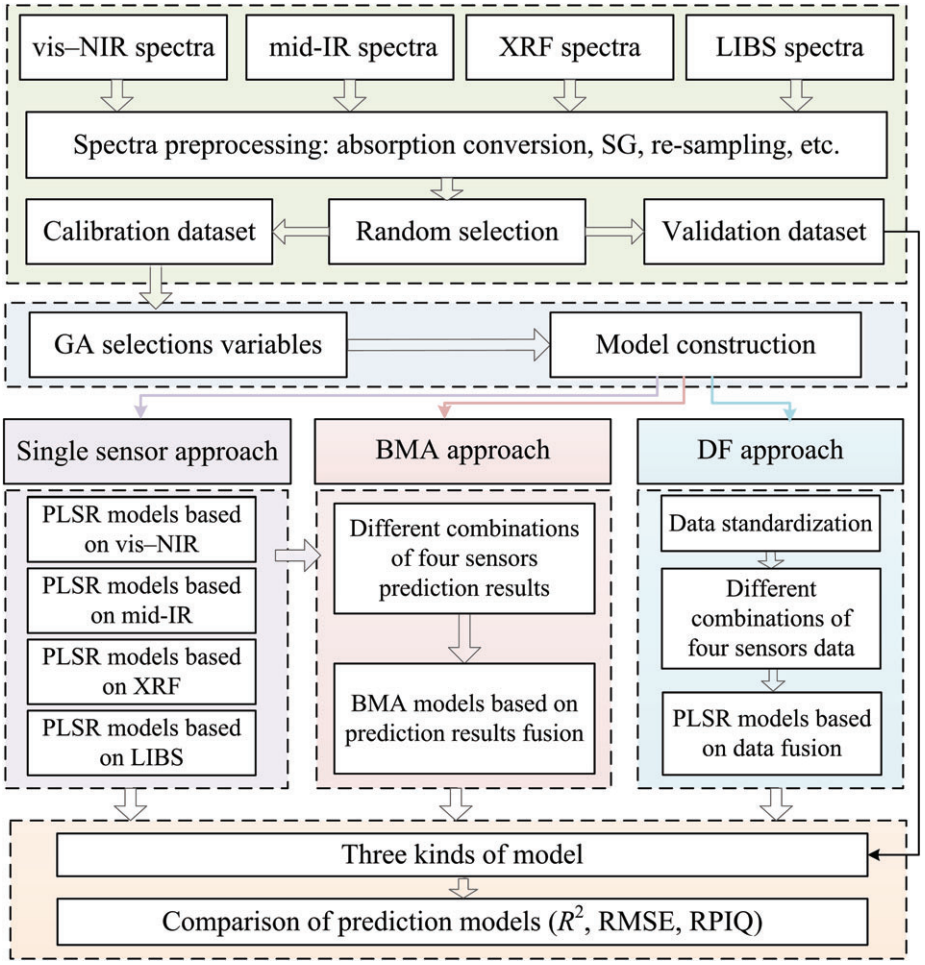

Figure 2 Flow chart of the chemometric analyses used to perform the predictions. XRF, X-ray fluorescence; LIBS, laser-induced breakdown spectroscopy; SG, Savitzky–Golay algorithm; GA, genetic algorithm; BMA, Bayesian model averaging; DF, data fusion; PLSR, partial least-squares regression; RMSE, root mean square error; RPIQ, ratio of performance to interquartile distance. [Colour figure can be viewed at wileyonlinelibrary.com].

Chemometric analyses

The outliers of soil samples might affect the accuracy of model prediction; thus, we identified outliers in both soil properties and the spectra using principal component analysis (PCA) and boxplots before the chemometric analysis. The spectra were pre-processed, and then we used a genetic algorithm and partial least-squares regression (GA–PLSR) to select characteristic bands for soil properties. We then created the prediction models using (i) the single sensor approach and (ii) the DF approach. Before data fusion, spectra from the four sensors were standardized to ensure the same orders of magnitude of the combined data. The standard normal variate (SNV) was calculated by subtracting the mean of the data from each value and dividing by its standard deviation in R package 'prospectr'. (iii) The BMA approach; the process is as shown in Figure 2.

Selection of characteristic bands with GA–PLSR. Selection of characteristic bands with strong information and insensitivity to external factors is an effective way to construct a robust model (Swierenga *et al.*, 2000). The four sensors all have large numbers of spectral bands and there is strong correlation between the numerous bands. It is necessary to select characteristic bands that can not only eliminate irrelevant or nonlinear variables and reduce redundancy, but also simplify the model to obtain a model with better prediction ability and that is more robust. As an optimization algorithm, GA has been widely used in the field of spectral analysis (Savvides *et al.*, 2010). In addition, PLSR was selected as the regression model for GA to obtain a more efficient and steadier model. The data were split randomly into a calibration dataset (two thirds) and a validation dataset (one third); a total of 10 random splits for calibration and validation datasets were made to improve the quality of the prediction results. Then the calibration data were used to select the characteristic bands for modelling using GA-PLSR. For this we used the PLS_Toolbox 8.5.1 (Eigenvector Research Inc., Wenatchee, WA, USA) in MatLab (The MathWorks Inc., Natick, MA, USA). The quality of the characteristic bands is affected directly by the window width. We tested several window widths, and after the calculations we set 5 as the window width for the four spectra. Moreover, to obtain a better representation of different variable combinations, the population size was set to 64 and each property was analysed five times.

The PLSR algorithm. The PLSR method is one of the most popular algorithms used for spectral calibration and prediction

among the multiple linear calibration algorithms (Wold *et al.*, 1983). This method has the advantage of eliminating the problem of multiple collinearities of the independent variables. Leave-one-out cross-validation was used to select the optimal number of PLSR latent variables to use in the model. For PLSR we used the R package 'pls' (Mevik & Wehrens, 2016) of R 3.3.3 (R Core Team, 2017).

The BMA algorithm. Combining different model outcomes is known as model averaging (Rojas *et al.*, 2008). In this study, model averaging was used to combine the single sensor predictions from the four sensors. The Bayesian model averaging (BMA) algorithm is a method of statistical analysis that considers the uncertainty of the model itself. First, we assume a linear relation between the four sensor predictions and the soil property of interest:

$$\mathbf{y} = \alpha + \mathbf{X}\,\beta + \xi \quad \xi \sim N\left(0,\ \sigma^2\right), \tag{1}$$

where **y** is the vector with the soil property of interest (dependent variable, $N \times 1$, N is the sample size), α is a constant, **X** is the independent variable matrix ($N \times m$, m is the variable number), β is the coefficient (m) and ξ is a normal IID error term with variance σ^2.

The parameters are estimated conditionally based on the measured values and the corresponding predictions from four single sensors by BMA. For more detail on the theory and algorithm of BMA, we refer the reader to Hoeting *et al.* (1999). The BMA was calculated with the R package 'BAS' (Clyde, 2017) of R 3.3.3 (R Core Team, 2017).

Model performance indices. The coefficient of determination (R^2), root mean square error (RMSE) and the ratio of performance to interquartile distance (RPIQ) were used to evaluate and compare the performance of the models:

$$R^2 = \frac{\sum_{i=1}^{N}\left(\hat{y}_i - \bar{y}_i\right)^2}{\sum_{i=1}^{N}\left(y_i - \bar{y}_i\right)^2}, \tag{2}$$

$$\mathrm{RMSE} = \sqrt{\frac{\sum_{i=1}^{N}\left(\hat{y}_i - y_i\right)^2}{N}}, \tag{3}$$

$$\mathrm{RPIQ} = \frac{Q_3 - Q_1}{\mathrm{RMSE}}, \tag{4}$$

where y_i is the i th observed value and $\hat{y}_i$ is the corresponding prediction, $\bar{y}_i$ is the mean of the observed values and N is the number of observations. The Q_1 is the first quartile and Q_3 is the third quartile. The larger are R^2 and RPIQ and the smaller is the RMSE, the better the model performance.

Results

Summary statistics and correlations among soil properties

Table 1 lists the summary statistics of the soil properties (after the removal of outliers). There were significant correlations ($P < 0.01$) among pH, SOM, TN and AN, and especially among SOM, TN and AN with $r > 0.9$ (Table 2). Correlations of AP with SOM, TN, AN and AK were also significant. Correlations of AK with other properties were weak, except for AP.

Characteristic bands extracted by GA–PLSR

Taking SOM as an example, the frequency of bands in the GA–PLSR resulting from the four sensors is shown in Figure 3, which clearly shows the important bands for each instrument. As shown in the vis–NIR plot, the high-frequency bands included in the GA selection models were 400–450, 900–950, 1350–1400, 1550–1600, 1875–1915, 2025–2075, 2175–2225 and 2225–2275 nm. For mid-IR, the high-frequency bands were around 3760–3680, 3280–3240, 3080–3040, 2920–2880, 2520–2440, 2200–2160, 1840–1800, 1760–1680, 1120–1080

Table 2 Lower triangular correlation matrix among six soil properties

Correlations	pH	SOM	TN	AN	AP	AK
pH	1.000					
SOM	0.323	1.000				
TN	0.337	**0.945**	1.000			
AN	0.336	**0.944**	**0.998**	1.000		
AP	−0.255	0.189	0.282	0.282	1.000	
AK	−0.117	−0.036	0.096	0.096	0.513	1.000

SOM, soil organic matter; TN, total nitrogen; AN, available nitrogen; AP, available phosphorus; AK, available potassium.

Table 1 Summary statistics of soil properties (SOM and TN in g kg^{-1}, other properties in mg kg^{-1})

Soil properties	Dataset	*N*	Min.	First Q.	Med.	Mean	Third Q.	Max.	Skew.
pH	Total	288	3.55	4.98	5.53	5.83	6.64	8.11	0.43
SOM	Total	294	8.70	24.40	29.90	30.75	36.50	78.10	0.88
TN	Total	288	0.07	0.15	0.18	0.19	0.22	0.47	0.87
AN	Total	288	6.36	12.03	13.90	14.40	16.64	33.56	0.87
AP	Total	291	1.70	13.05	29.45	125.2	82.42	1982.1	3.58
AK	Total	294	29.00	72.00	96.00	141.9	156.0	1630.0	4.95

N, sample size; Min., minimum; Q., quartile; Med., median; Max., maximum; Skew., skewness; SOM, soil organic matter; TN, total nitrogen; AN, available nitrogen; AP, available phosphorus; AK, available potassium.

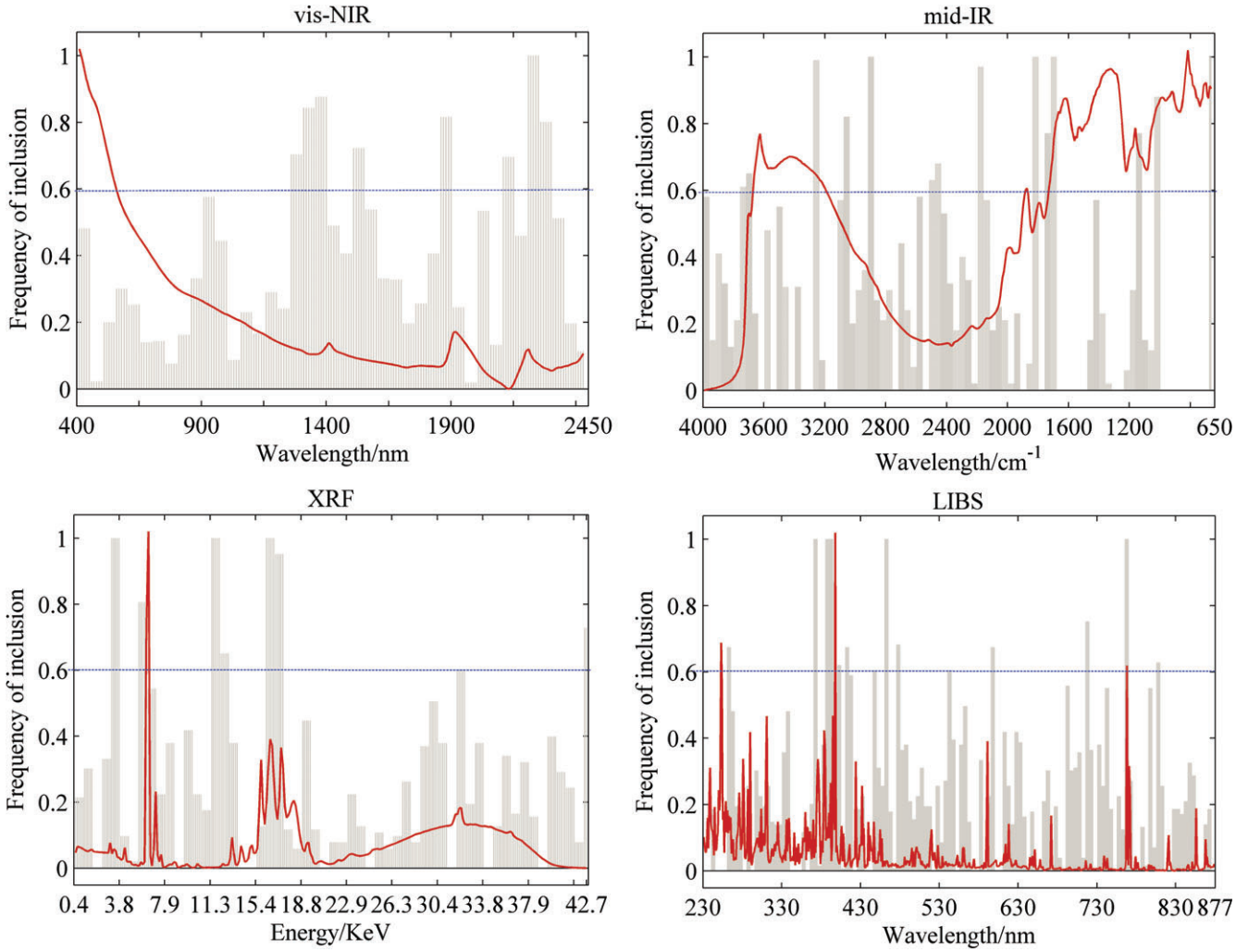

Figure 3 Frequency of bands in the models and the average spectrum (red line) of the four instruments (taking soil organic matter [SOM] as an example). XRF, X-ray fluorescence; LIBS, laser-induced breakdown spectroscopy. [Colour figure can be viewed at wileyonlinelibrary.com].

and 1040–1000 cm^{-1}. The high-frequency XRF bands were located around 3.4–4.15, 5.65–7.15, 11.65–13.15, 15.15–16.65 and 30.9–31.65 keV. For LIBS, the high-frequency bands were located at 260–270, 370–375, 385–395, 400–405, 410–420, 445–450, 460–465, 475–480, 540–545, 560–565, 595–600, 715–720, 765–770 and 805–810 nm. The results of root mean square error of cross-validation (RMSECV) for each model are shown in Figure 4. The red dot is the model selected by GA–PLSR. As Figure 4 shows, GA–PLSR selects the model with the smallest RMSECV. The number of bands chosen for pH, SOM, TN, AN, AP and AK based on vis–NIR were 45, 60, 75, 73, 58 and 55, respectively.

Prediction using the single sensor approach

Figure 5 shows the average R^2 of cross-validation and validation over 10 random splits of the data into calibration and validation datasets; the results of cross-validation and validation were similar. Figure 6 shows the indices of model performance for the six soil properties using the single sensor approach. For pH, SOM, TN and AN, the most accurate predictions were from the mid-IR spectra ($R^2 > 0.75$ and RPIQ > 2.5), then from the vis–NIR spectra. The models from LIBS spectra for pH, SOM, TN and AN were moderately accurate (R^2 of 0.63–0.71 and RPIQ > 2.0). In contrast, the models from PXRF spectra for these four soil properties were poor and could not be used separately. The best models for AP and AK were from vis–NIR spectra with R^2 of 0.39 and 0.27 and RPIQ of 1.64 and 1.39, respectively.

In general, pH, SOM, TN and AN could be predicted well by vis–NIR or mid-IR spectra. However, the predictions for AP and AK based on the single sensor were poor. On the whole, the predictive ability of the sensor for the soil properties studied was in the order mid-IR > vis–NIR > LIBS > XRF.

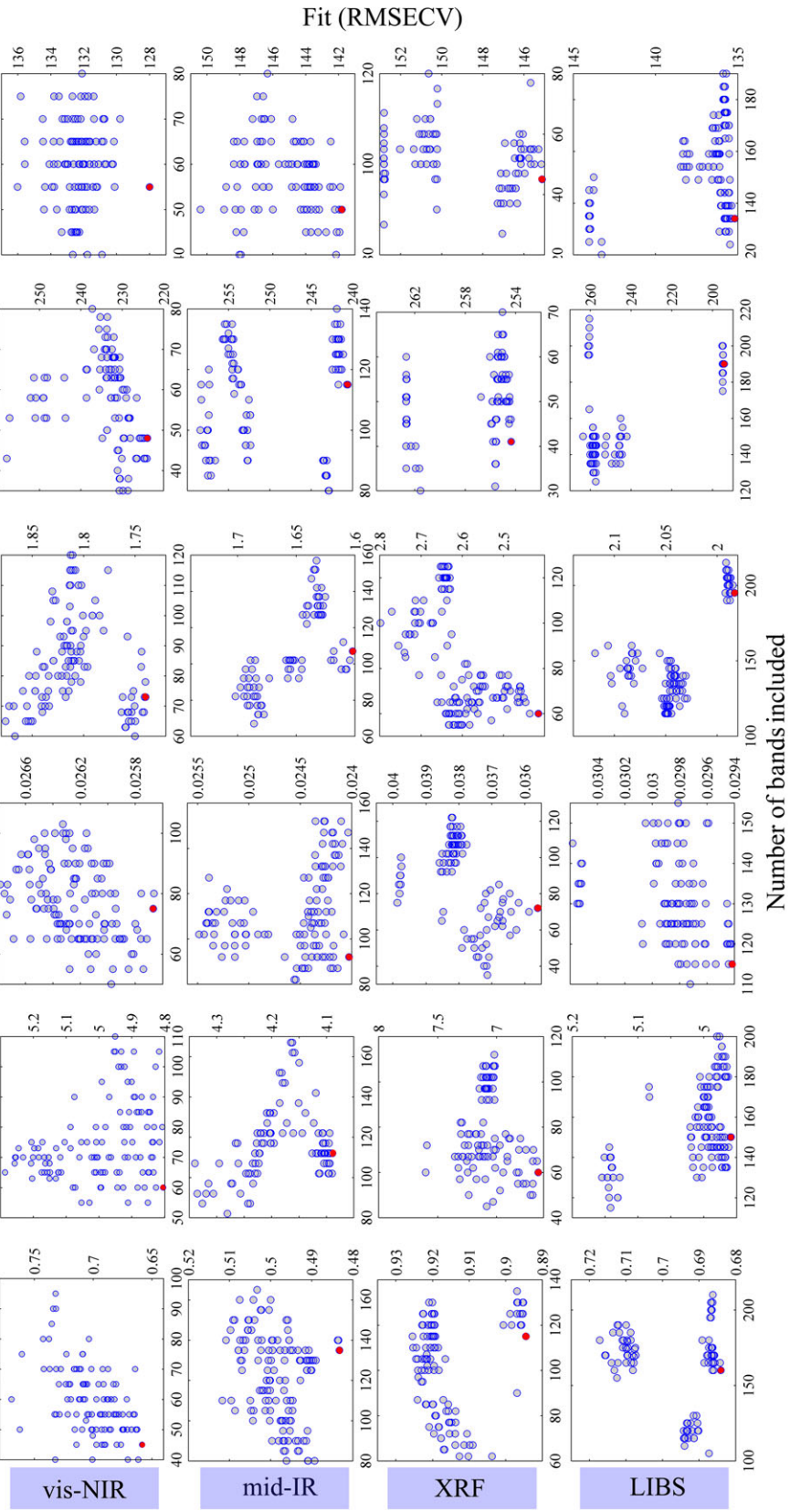

Figure 4 The root mean square error of cross-validation (RMSECV) of regression models in the genetic algorithm (GA) process plotted against number of bands included in the models for six properties. XRF, X-ray fluorescence; LIBS, laser-induced breakdown spectroscopy. [Colour figure can be viewed at wileyonlinelibrary.com].

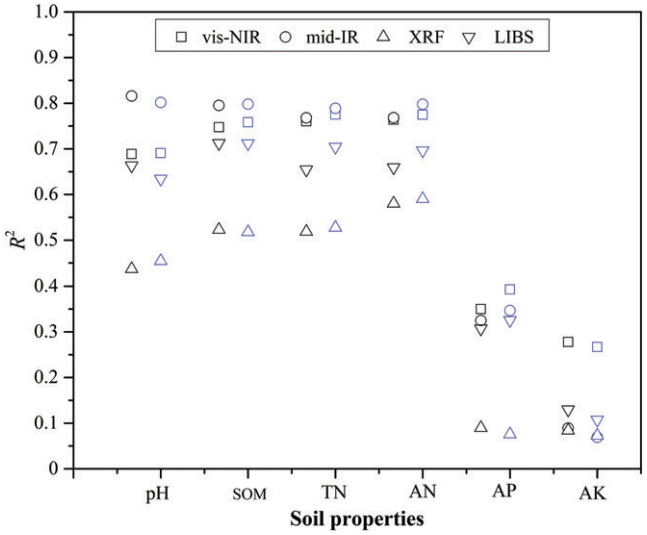

Figure 5 The coefficient of determination, R^2, plotted against cross-validation (black symbols) and validation (blue symbols) of the six soil properties. XRF, X-ray fluorescence; LIBS, laser-induced breakdown spectroscopy; SOM, soil organic matter; TN, total nitrogen; AN, available nitrogen; AP, available phosphorus; AK, available potassium. [Colour figure can be viewed at wileyonlinelibrary.com].

Prediction using the data fusion (DF) approach

The prediction results of soil properties based on the DF approach are shown in Figure 7. For pH, the best combination was the fusion of vis–NIR and mid-IR, with R^2 of 0.81 and RPIQ of 3.17. However, compared with the best prediction based on the single sensor, there was no obvious improvement for pH. The best combination for SOM was the fusion of mid-IR and LIBS data, with R^2 of 0.81 and RPIQ of 2.99. This was slightly better than the best prediction based on mid-IR data alone. The best combinations for TN and AN were the fusion of vis–NIR, mid-IR and PXRF with R^2 of 0.81 and RPIQ of 2.79 and 2.81, respectively. The best combination for AP was the fusion of vis–NIR, mid-IR and LIBS with R^2 of 0.48 and RPIQ of 1.79, whereas for AK, it was the fusion of vis–NIR, mid-IR and XRF data with R^2 of 0.19 and RPIQ of 1.33. However, the prediction accuracy for AP and AK based on data fusion remained poor. For AK, in particular, the prediction accuracy was even weaker than for single sensors.

Prediction using the BMA approach

Figure 8 shows the indices of model performance for the six soil properties using the BMA approach. Compared with the single sensor and DF approaches, the BMA approach improved the prediction accuracy of all six soil properties. Particularly satisfactory results were achieved for SOM, TN and AN with $R^2 > 0.85$ and RPIQ > 3.0. The model average of vis–NIR and mid-IR produced the best prediction for pH ($R^2 = 0.83$ and RPIQ = 3.38). For SOM, TN and AN, the model average of vis–NIR, mid-IR and LIBS achieved the best prediction with R^2 of 0.86, 0.87 and 0.87, respectively, and RPIQ of 3.41, 3.36 and 3.33, respectively. For AP, the best model average was from vis–NIR and mid-IR with R^2 of 0.47 and RPIQ of 1.77. For AK, the best model average was based on the outcomes of vis–NIR, XRF and LIBS with R^2 of 0.28 and RPIQ of 1.77. Although the model averages for AP and AK were better than for a single sensor or sensor data fusion, the prediction accuracy remained poor.

Discussion

To compress the input data from the four sensors, thus reducing the amount of computation and model complexity, we first used GA–PLSR to select characteristic bands. The GA–PLSR simplified the models by selecting meaningful bands that produced the smallest RMSECV, whereas the full set of bands contained a great deal of redundant information (Wang *et al.*, 2014).

The spectral characteristics of SOM in the vis–NIR spectra were mainly derived from C–H, C–O, C=O and N–H bonds with their vibrations of the fundamental frequency and frequency multiplication. As previous studies have shown, the characteristic bands of C–H may be around 825, 853, 877, 1100, 1138, 1170, 1650, 1730–1852, 2275 and 2307–2469 nm. For C–O, the characteristic bands are 1961, 2137 and 2381 nm. For C=O, the characteristic bands are mainly at 1499, 1524, 1930 and 2033 nm. Finally, 751, 1000, 1500 and 2060 nm might be the characteristic bands for N–H (Viscarra Rossel *et al.*, 2006). In the current study, the meaningful bands for SOM were mainly located around 425, 900, 1400, 1525, 1900, 2025, 2125, 2275 and 2300 nm. The bands around 900, 2275 and 2300 nm might be affected by C–H, 2125 nm might be affected by C–O, bands around 1525 and 2025 might be affected by C=O and bands around 425 nm might be affected by electron transition of iron oxides. Bands around 1400 nm represent the moisture absorption zone, and the high frequency in this band is mainly a result of the hygroscopic effect of SOM. The bands around 820, 1100, 1400, 1430, 1600, 1630, 1700–1800, 1930, 2000, 2100 and 2200–2400 nm are important for the prediction of SOM and TN (Stenberg *et al.*, 2010). There were more high-frequency bands in mid-IR than vis–NIR because of the strong vibration of chemical groups (Figure 3). Bands around 3680 and 2920 cm^{-1} are related to the stretching vibrations of O–H, C–H and N–H, bands near 2440 cm^{-1} might be affected by C–OH, bands around 1800 cm^{-1} mainly relate to SiO_2, bands around 1680 cm^{-1} might be related to the stretching vibrations of C=O, C=C and C–N and the bending vibration of N–H, and bands around 1040 cm^{-1} mainly relate to the stretching vibration of C–O (Baes & Bloom, 1989).

For single sensors, the prediction accuracy based on vis–NIR, mid-IR, PXRF and LIBS varied for different soil properties. The most accurate predictions for pH, SOM, TN and AN were obtained from mid-IR (Viscarra Rossel *et al.*, 2006; Chen *et al.*, 2016). The vis–NIR model performed best for AP and AK. Taken together, the predictive ability for these soil properties was mid-IR > vis–NIR > LIBS> PXRF. Among these properties, pH, SOM, TN and AN can be characterized quantitatively by vis–NIR or mid-IR. The successful predictions by vis–NIR were mainly

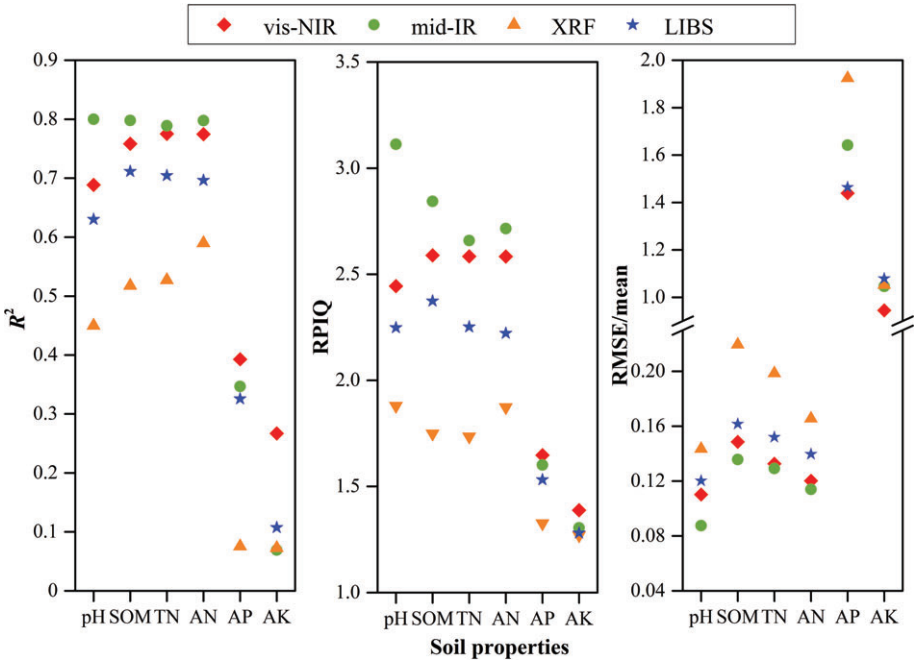

Figure 6 Model performance statistics of validation set plotted against the six soil properties using single sensor data. XRF, X-ray fluorescence; LIBS, laser-induced breakdown spectroscopy; RPIQ, ratio of performance to interquartile distance; RMSE, root mean square error. [Colour figure can be viewed at wileyonlinelibrary.com].

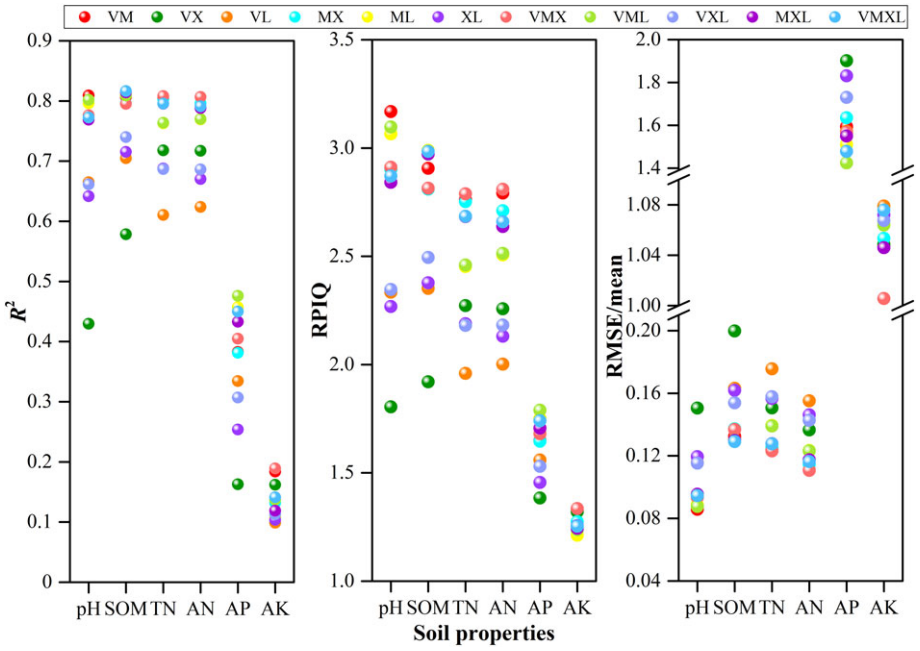

Figure 7 Model performance statistics of validation set plotted against the six soil properties using the data fusion approach (V, vis–NIR; M, mid-IR; X, portable X-ray fluorescence [PXRF]; L, laser-induced breakdown spectroscopy [LIBS]; for example, VM represents the fusion of vis–NIR and mid-IR spectra, and so on). RPIQ, ratio of performance to interquartile distance; RMSE, root mean square error; SOM, soil organic matter; TN, total nitrogen; AN, available nitrogen; AP, available phosphorus; AK, available potassium. [Colour figure can be viewed at wileyonlinelibrary.com].

related to vibrations of molecular bonds such as O–H, N–O, N–H, C–H + C–H, C–H + C–C, C=O and C=C in the vis–NIR spectra (Stenberg *et al.*, 2010). Although there were no direct spectral responses of pH in the vis–NIR spectra, the prediction accuracy of pH was very good because of its relation to the wavelengths of organic material, iron oxides and clay minerals (Kuang *et al.*, 2012). In the mid-IR, in response to the strong fundamental vibrations, soil spectra were characterized by clearly identifiable peaks linked to organic or mineral compounds and thus provided better predictions (Nocita *et al.*, 2015). Although PXRF and LIBS do not measure these soil properties directly, previous research has shown that other elements have strong associations with these soil properties (Sharma *et al.*, 2014). Therefore, we integrated multiple sensors for further prediction.

Data fusion or synergistic use of multi-sensor spectra could increase the capacity for the prediction of soil properties (O'Rourke *et al.*, 2016). With the fusion of spectra from the four instruments, there were slight improvements in the prediction of

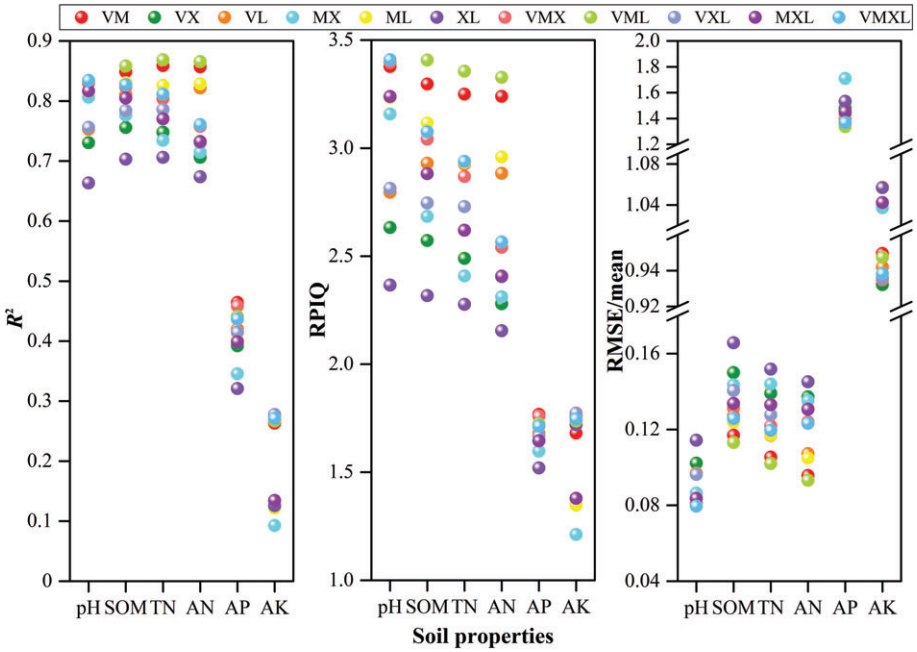

Figure 8 Model performance statistics of validation set plotted against the six soil properties using the Bayesian model averaging (BMA) approach (V, vis–NIR; M, mid-IR; X, portable X-ray fluorescence [PXRF]; L, laser-induced breakdown spectroscopy [LIBS]; for example, VM represents the fusion of vis–NIR and mid-IR spectra, and so on). RPIQ, ratio of performance to interquartile distance; RMSE, root mean square error; SOM, soil organic matter; TN, total nitrogen; AN, available nitrogen; AP, available phosphorus; AK, available potassium. [Colour figure can be viewed at wileyonlinelibrary.com].

SOM, TN and AN, which might be a result of the covariation of non-chromophores or spectrally inactive components (PXRF elements or LIBS elements) with relevant chromophores or spectrally active components, especially organic carbon (Wang *et al.*, 2015). As shown in previous research, better predictions of several soil properties can be achieved by integrating spectra from different sensors. However, we found that the prediction accuracy for pH and AK was no better, or even poorer, than that based on single sensors, which might have resulted from a large amount of redundancy in the combined spectra.

Model averaging nearly always improves model predictive accuracy and rarely makes worse predictions than single sensor models (Abbott, 2014). The BMA models for pH, SOM, TN and AN were better than those using single or fused sensor data as input, and achieved satisfactory results ($R^2 > 0.83$ and RPIQ > 3.0). However, for AP and AK, although the BMA models improved the accuracy of prediction, the models were still poor ($R^2 < 0.5$, RPIQ < 2.0). Moreover, the prediction results of TN and AN based on single sensor, sensor data fusion and BMA were similar because AN has a strong correlation with TN (Table 2). This might also explain why AN can be predicted well. Model averaging of vis–NIR or mid-IR with other auxiliary sensors such as PXRF or LIBS could improve the accuracy of prediction of these six pivotal properties for evaluating soil fertility.

In this study, we aimed to explore the possibility of combining different sensors for predicting several soil properties under laboratory conditions. Compared with single sensor models, the BMA model produced the best predictions, especially for the properties with small and large values (Figure 9). Nevertheless, using integration of several soil sensors in the field is our final goal. Several attempts to use vis–NIR spectroscopy in the field have been reported (Li *et al.*, 2015). Recently, portable, easy to use, non-destructive and field-use mid-IR analysers have been developed, such as the Agilent hand-held FTIR, and researchers have also started to use the portable mid-IR spectrometer for field assessment of soil properties (Ji *et al.*, 2016). In addition, PXRF and LIBS have also been used under field conditions (Peinado *et al.*, 2010; Bricklemyer *et al.*, 2011). With the development of sensors, there is an increasing number of soil sensing platforms (Viscarra Rossel *et al.*, 2017). The field use of the single instrument and various integrated platforms provides the possibility of sensor fusion directly in the field, but there are more uncertainties for field measurement because of the complex nature of soil. Thus, it is important to study sensor fusion under field conditions and our research provides the basic study for field application.

Conclusions

In this study, we integrated four proximal sensors to determine soil properties. The results of this study indicated the following. (i) The predictive capability of the four sensors for these soil properties decreased as follows: mid-IR > vis–NIR > LIBS > XRF. (ii) Fusion of the spectra obtained with the four sensors resulted in a slight improvement of the predictions of SOM, TN, AN and AP, whereas the results for pH and AK were comparable or even poorer. The DF approach was discarded because it caused a large amount of redundancy and increased the complexity of computation while producing no obvious improvement in the determination of soil properties. (iii) Compared with the single sensor and DF approaches, the BMA approach improved the prediction accuracy of six properties. For the prediction of the above six properties, PXRF was not of benefit and should be discarded. In conclusion, model averaging of vis–NIR, mid-IR and LIBS could be a stable and reliable replacement for traditional methods for the prediction of soil properties.

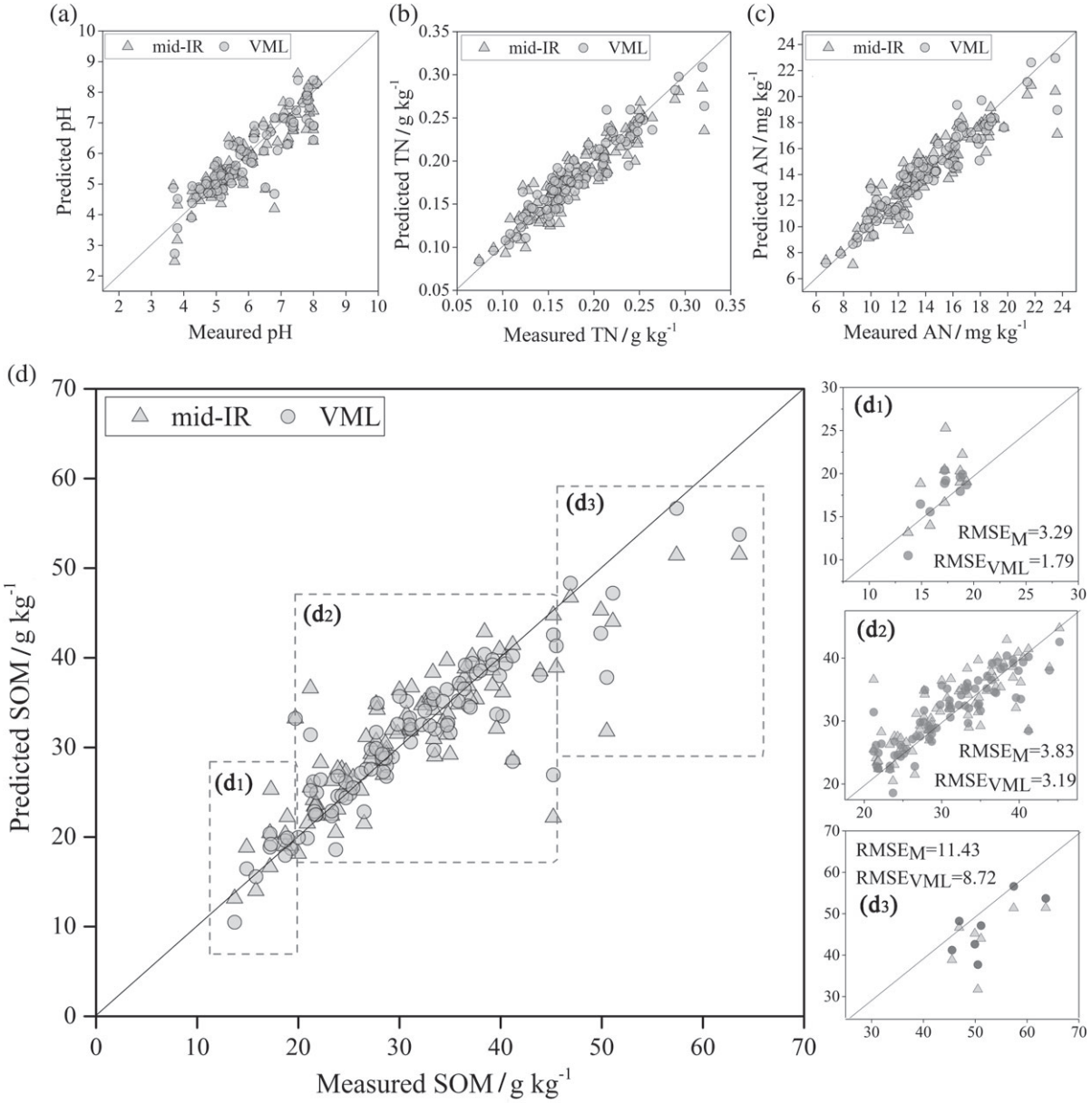

Figure 9 Measured values plotted against predicted values of the validation data based on the best single sensor and the best combination of Bayesian model averaging (BMA) ((a), (b), (c) and (d) show the full validation of pH, TN, AN and SOM, respectively; (d_1), (d_2), (d_3) show the detailed information of SOM (<25, 25–45, >45 g kg^{-1})) (M, mid-IR; VML, the fusion of vis–NIR, mid-IR and laser-induced breakdown spectroscopy [LIBS]). TN, total nitrogen; AN, available nitrogen; SOM, soil organic matter; RMSE, root mean square error.

Acknowledgements

We thank the National Key Research and Development Program (2017YFD0700501) and Public Projects of Zhejiang Province (LGN18D010003) for support.

References

Abbott, D. 2014. *Applied Predictive Analytics. Principles and Techniques for the Professional Data Analyst*. John Wiley & Sons Inc., Indianapolis, IN.

Baes, A.U. & Bloom, P.R. 1989. Diffuse reflectance and transmission fourier-transform infrared (drift) spectroscopy of humic and fulvic-acids. *Soil Science Society of America Journal*, **53**, 695–700.

Bao, S.D. 1981. *Soil and Agricultural Chemistry Snalysis*. ChinaAgricultural Press, Beijing.

Bricklemyer, R.S., Brown, D.J., Barefield, J.E. & Clegg, S.M. 2011. Intact soil core total, inorganic, and organic carbon measurement using laser-induced breakdown spectroscopy. *Soil Science Society of America Journal*, **75**, 1006–1018.

Chen, S.C., Peng, J., Ji, W.J., Zhou, Y., He, J.X. & Shi, Z. 2016. Study on the characterization of VNIR-MIR spectra and prediction of soil

organic matter in paddy soil. *Spectroscopy and Spectral Analysis*, **36**, 1712–1716.

Clyde, M. 2017. *BAS: Bayesian Adaptive Sampling for Bayesian Model Averaging*. R package version 1.4.6. [WWW document]. URL https://CRAN.R–project.org/web/packages/BAS [accessed on 26 May 2017].

Gebbers, R. & Adamchuk, V.I. 2010. Precision agriculture and food security. *Science*, **327**, 828–831.

Guo, J.H., Liu, X.J., Zhang, Y., Shen, J.L., Han, W.X. & Zhang, W.F. 2010. Significant acidification in major Chinese croplands. *Science*, **327**, 1008–1010.

Hoeting, J.A., Madigan, D., Raftery, A.E. & Volinsky, C.T. 1999. Bayesian model averaging: a tutorial. *Statistical Science*, **14**, 382–401.

Hu, B.F., Chen, S.C., Hu, J., Xia, F., Xu, J.F. & Li, Y. 2017. Application of portable XRF and VNIR sensors for rapid assessment of soil heavy metal pollution. *PLoS One*, **12**, e0172438.

Ji, W.J., Adamchuk, V.I., Biswas, A., Dhawale, N.M., Sudarsan, B. & Zhang, Y.K. 2016. Assessment of soil properties in situ using a prototype portable MIR spectrometer in two agricultural fields. *Biosystems Engineering*, **152**, 14–27.

Knadel, M., Gislum, R., Hermansen, C., Peng, Y., Moldrup, P. & de Jonge, L.W.H. 2017. Comparing predictive ability of laser-induced breakdown spectroscopy to visible near–infrared spectroscopy for soil property determination. *Biosystems Engineering*, **156**, 157–172.

Kuang, B., Mahmood, H.S., Quraishi, M.Z., Hoogmoed, W.B., Mouazen, A.M. & van Henten, E.J. 2012. Sensing soil properties in the labotary, in situ, and on-line: a review. *Advances in Agronomy*, **114**, 155–223.

Li, Q. 1992. *Paddy Soils of China*. Science Press, Beijing.

Li, S., Shi, Z., Chen, S.C., Ji, W.J., Zhou, L.Q. & Yu, W. 2015. In situ measurements of organic carbon in soil profiles using vis–NIR spectroscopy on the Qinghai-Tibet Plateau. *Environmental Science & Technology*, **49**, 4980–4987.

Mevik, B.H. & Wehrens, R. 2016. *pls: Partial Least Squares and* Principal *Component Regression*. R package version 2.6–0 [WWW document]. URL https://CRAN.R–project.org/package=pls [accessed on 18 December 2016].

Miller, R.W. & Gardiner, D.T. 1998. *Soils in Our Environment*. Prentice Hall, Upper Saddle River, NJ.

Nocita, M., Stevens, A., van Wesemael, B., Aitkenhead, M., Bachmann, M. & Barthès, B. 2015. Soil spectroscopy: an alternative to wet chemistry for soil monitoring. *Advances in Agronomy*, **132**, 139–159.

O'Rourke, S.M., Stockmann, U., Holden, N.M., McBratney, A.B. & Minasny, B. 2016. An assessment of model averaging to improve predictive power of portable vis–NIR and XRF for the determination of agronomic soil properties. *Geoderma*, **279**, 31–44.

Peinado, F.M., Ruano, S.M., Gonzalez, M.G.B. & Molina, C.E. 2010. A rapid field procedure for screening trace elements in polluted soil using portable X-ray fluorescence (PXRF). *Geoderma*, **159**, 76–82.

R Core Team 2017. *R: A* Language *and* Environment *for Statistical* Computing. R Foundation for Statistical Computing, Vienna [WWWdocument]. URL https://www.R–project.org/ [accessed on 6 March 2017].

Rojas, R., Feyen, L. & Dassargues, A. 2008. Conceptual model uncertainty in groundwater modeling: combining generalized likelihood uncertainty estimation and Bayesian model averaging. *Water Resources Research*, **44**, W12418. https://doi.org/10.1029/2008WR006908.

Samek, O., Lambert, J., Hergenroder, R., Liska, M., Kaiser, J. & Novotny, K. 2006. Femtosecond laser spectrochemical analysis of plant samples. *Laser Physics Letters*, **3**, 21–25.

Santos, D., Nunes, L.C., Trevizan, L.C., Godoi, Q., Leme, F.O. & Braga, J.W.B. 2009. Evaluation of laser induced breakdown spectroscopy for cadmium determination in soils. *Spectrochimica Acta Part B–Atomic Spectroscopy*, **64**, 1073–1078.

Savitzky, A. & Golay, M.J.E. 1964. Smoothing and differentiation of data by simplified least squares procedures. *Analytical Chemistry*, **36**, 1627–1639.

Savvides, A., Corstanje, R., Baxter, S.J., Rawlins, B.G. & Lark, R.M. 2010. The relationship between diffuse spectral reflectance of the soil and its cation exchange capacity is scale-dependent. *Geoderma*, **154**, 353–358.

Sharma, A., Weindorf, D.C., Man, T., Aldabaa, A.A.A. & Chakraborty, S. 2014. Characterizing soils via portable X-ray fluorescence spectrometer: 3. Soil reaction (pH). *Geoderma*, **232**, 141–147.

Soil Science Society of China 2000. *Soil and Agricultural Chemistry Analysis*. China Agricultural Science and Technology, Beijing.

Stenberg, B., Viscarra Rossel, R.A., Mouazen, A.M. & Wetterlind, J. 2010. Visible and near infrared spectroscopy in soil science. *Advances in Agronomy*, **107**, 163–215.

Swierenga, H., Wulfert, F., de Noord, O.E., de Weijer, A.P., Smilde, A.K. & Buydens, L.M.C. 2000. Development of robust calibration models in near infra–red spectrometric applications. *Analytica Chimica Acta*, **411**, 121–135.

Villas-Boas, P.R., Romano, R.A., Franco, M.A.D., Ferreira, E.C., Ferreira, E.J. & Crestana, S. 2016. Laser-induced breakdown spectroscopy to determine soil texture: a fast analytical technique. *Geoderma*, **263**, 195–202.

Viscarra Rossel, R.A. & Webster, R. 2012. Predicting soil properties from the Australian soil visible–near infrared spectroscopic database. *European Journal of Soil Science*, **63**, 848–860.

Viscarra Rossel, R.A., Walvoort, D.J.J., McBratney, A.B., Janik, L.J. & Skjemstad, J.O. 2006. Visible, near infrared, mid infrared or combined diffuse reflectance spectroscopy for simultaneous assessment of various soil properties. *Geoderma*, **131**, 59–75.

Viscarra Rossel, R.A., Lobsey, C.R., Sharman, C., Flick, P. & McLachlan, G. 2017. Novel proximal sensing for monitoring soil organic C stocks and condition. *Environmental Science & Technology*, **51**, 5630–5641.

Wang, S.Q., Li, W.D., Li, J. & Liu, X.S. 2013. Prediction of soil texture using FT-NIR spectroscopy and PXRF spectrometry with data fusion. *Soil Science*, **178**, 626–638.

Wang, J., Cui, L., Gao, W., Shi, T., Chen, Y. & Gao, Y. 2014. Prediction of low heavy metal concentrations in agricultural soils using visible and near-infrared reflectance spectroscopy. *Geoderma*, **216**, 1–9.

Wang, D., Chakraborty, S., Weindorf, D.C., Li, B., Sharma, A. & Paul, S. 2015. Synthesized use of VisNIR DRS and PXRF for soil characterization: Total carbon and total nitrogen. *Geoderma*, **243–244**, 157–167.

Wold, S., Martens, H. & Wold, H. 1983. The multivariate calibration-problem in chemistry solved by the PLS method. *Lecture Notes in Mathematics*, **973**, 286–293.

Xu, D., Ma, W., Chen, S., Jiang, Q., He, K. & Shi, Z. 2018. Assessment of important soil properties related to Chinese soil taxonomy based on vis–NIR reflectance spectroscopy. *Computers and Electronics in Agriculture*, **144**, 1–8.

Zhou, Y., Biswas, A., Ma, Z., Lu, Y., Chen, Q. & Shi, Z. 2016. Revealing the scale-specific controls of soil organic matter at large scale in Northeast and North China Plain. *Geoderma*, **271**, 71–79.

Zhu, Y.D., Weindorf, D.C. & Zhang, W.T. 2011. Characterizing soils using a portable X-ray fluorescence spectrometer: 1. Soil texture. *Geoderma*, **167–168**, 167–177.